Biomedicine & Pharmacotherapy 117 (2019) 109091

Contents lists available at ScienceDirect

Biomedicine & Pharmacotherapy

journal homepage: www.elsevier.com/locate/biopha

Diosmetin inhibits tumor development and block tumor angiogenesis in skin cancer

Jawun Choi, Dae-Hyo Lee, Sang-Youel Park, Jae-Won Seol*

College of Veterinary Medicine, Chonbuk National University, Iksan, Jeollabuk-do 54596, Republic of Korea

ARTICLE INFO

Keywords:
Diosmetin
Melanoma
Tumor angiogenesis
angiopoietin-2
Metastasis

ABSTRACT

Diosmetin is a natural flavonoid obtained from citrus fruits and some medicinal herbs. Previous studies have reported the anti-cancer activity of diosmetin in some types of tumors. However, it is still unclear whether diosmetin exerts anti-cancer effects, particularly anti-angiogenic effects, in skin cancer. In this study, we used B16F10 melanoma cells and human umbilical vein endothelial cells to investigate the inhibitory effect of diosmetin on cell proliferation, migration and tube formation *in vitro*. Rat aorta ring assays were performed to determine the effect of diosmetin on ECs sprouting *ex vivo*. Furthermore, a B16F10 mouse melanoma model was used to observe the effect of diosmetin on tumor growth, angiogenesis, and metastasis *in vivo*. Our results showed that diosmetin not only suppressed tumor cell proliferation and migration but also induced cell apoptosis *via* the caspase pathway in B16F10 cells, and potently inhibited tube formation and cell migration in HUVECs. Rat aorta ring assays showed that diosmetin attenuated the ECs sprouting. Moreover, the mouse melanoma model showed that diosmetin significantly delayed tumor growth by inhibiting tumor vessels sprouting and expansion during tumor progression. Notably, diosmetin induced the normalization of tumor vasculature through the down-regulation of angiopoietin-2 and the improvement of pericyte coverage, leading to suppression of metastasis formation in lungs and lymph nodes. In conclusion, our results demonstrate that diosmetin suppresses tumor progression and metastasis by inducing tumor cell death and inhibiting tumor angiogenesis as well as normalizing the defective tumor vasculature, suggesting that diosmetin is a potential adjuvant chemotherapy agent.

1. Introduction

Malignant melanoma is the most lethal form of skin cancer, accounting for approximately 90% of the deaths caused by this disease [1,2]. In recent decades, the incidence of melanoma has steadily risen. Worldwide, there were about 55,000 deaths in 2012 [3] and according to the International Agency for Research on Cancer, in 2030, an estimated 351,396 new cases and 87,725 deaths are expected to occur [4]. The aggressiveness of melanoma is associated with its high metastatic potential [5]. If recognized during the early stages, melanoma can be removed by surgical excision. However, once it metastasizes, it is difficult to treat and has poor prognosis.

Chemotherapy is the most commonly chosen treatment option for the management of melanoma that has disseminated. In general, however, the current chemotherapies to treat melanoma have low efficacy and cause severe adverse effects [6]. Therefore, the development of anti-cancer drug that are both effective and safe is urgently required.

Diosmetin, the aglycone part of the flavonoid glycosides diosmin, is abundant in citrus fruits, oregano and is also obtained from some medicinal herbs such as *Rosa agrestis* Savi (Rosaceae) and *Anastatica hierochuntica* L. (Brassicaceae) [7–10]. Several therapeutic activities of diosmetin, such as antibacterial, anti-inflammatory, and antioxidant properties, have been reported [11–13]. It has been also demonstrated that diosmetin has a potent anti-proliferative effect in some tumor cells, including MDA-MB 468 breast cancer cells [14], uterine cervical carcinoma cells injected in mice [15], and HepG2 hepatocellular carcinoma cells [16,17]. However, the therapeutic activity of diosmetin in malignant melanoma is still unknown.

Angiogenesis, the formation of new vasculature through the sprouting and extension from pre-existing vessels, occurs in several pathological conditions including various malignant solid tumors [18,19]. In tumor progression, tumor-induced angiogenesis supplies nutrients and oxygen and removes metabolites, resulting in further tumor growth [20]. Moreover, tumor vasculature is one of the routes to the spreading of tumor cells to distant organs [21]. Therefore, inhibition of tumor-induced angiogenesis has become a promising strategy for cancer therapy. On the other hand, tumor blood vessels have impaired structure and functionality [21–24]. The defective tumor vascular

* Corresponding author.
E-mail address: jwsseol@jbnu.ac.kr (J.-W. Seol).

https://doi.org/10.1016/j.biopha.2019.109091
Received 22 March 2019; Received in revised form 2 June 2019; Accepted 4 June 2019

network severely delays blood perfusion into and from the tumor [23,25], and often generates an extremely hypoxic and acidic microenvironment, which leads to increased drug resistance and dissemination to distant tissues [26,27]. Thereby, increasing attention has been focused on "tumor vessel normalization", a process that could reconstruct the structurally and functionally defective tumor vasculature [28,29]. The normalization of tumor vascular network might increase tumor blood flow, eventually leading to enhanced chemotherapeutic efficacy [30].

Therefore, in this study, we aimed to investigate whether diosmetin possesses the anti-cancer effect in melanoma, particularly on tumor angiogenesis. We used B16F10 cells, human umbilical vein endothelial cells (HUVECs), and rat aorta to examine the effect of diosmetin *in vitro* and *ex vivo*. Furthermore, we confirmed effect of diosmetin on tumor growth, vasculature, and metastasis in a mouse melanoma model.

2. Materials and methods

2.1. Mice

All animal experiments were performed with approval (CBNU 2018-024) from the Animal Care Committee of Chonbuk National University. Specific pathogen-free C57BL/6 mice were purchased from Samtako Bio Korea Co., ltd. (Osan, Korea). All mice were fed with *ad libitum* access to a standard diet (PMI Lab diet, Richmond, IN, USA) and water.

2.2. Tumor model and diosmetin-treatment

B16F10 melanoma cells were obtained from the Korean Cell line Bank (Seoul, Korea). To generate implantation melanoma model, suspensions of B16F10 cells (1×10^6 cells in 100 μl) were subcutaneously injected into the dorsal flank of seven-week old mice and the mice were divided in two groups: untreated(n = 16) and diosmetin-treated (n = 16). Tumor volume and tumor growth rate were measured using previously reported methods [13]. Indicated days later, the mice were sacrificed by cervical dislocation and tissues were harvested fro further analyses. Diosmetin (1.0 mg/kg two times every day, Sigma-Aldrich, St. Louis, MO, USA) was intraperitoneally injected for two weeks from seven days after tumor implantation. As a control, equal amounts of PBS were injected in the same manner.

2.3. Histological analysis

For hematoxylin and eosin (H&E) staining, lung tissues were fixed overnight in 4% paraformaldehyde. After tissue processing using standard procedures, samples were embedded in paraffin, and cut into 5-μm sections followed by H&E staining. For immunofluorescence studies, tumor tissues and inguinal lymph nodes (ILNs) were fixed in 4% paraformaldehyde for 4 h, dehydrated in 20% sucrose solution overnight, and embedded in tissue freezing medium (Leica, Wetzlar, Germany). Frozen blocks were cut into 50-μm sections. The sectioned samples were blocked with 5% donkey (or goat) serum in 0.3% Triton X-100 in phosphate-buffered saline (PBS) for 3 h at room temperature (RT) and then incubated overnight at 4 °C with the following primary antibodies: anti-CD31 (hamster, clone 2H8; Millipore Billerica, MA, USA), FITC-conjugated anti-alpha-smooth muscle actin (α-SMA) (mouse, clone 1A4; Sigma-Aldrich), anti-caspase-3 (rabbit polyclonal; R&D Systems, Minneapolis, MN, USA), anti-LYVE-1 (rabbit polyclonal; AngioBio, Del Mar, CA, USA), anti-pan-cytokeratin (mouse, clone AE1/AE3; Abcam, Cambridge, MA, USA), and anti-angiopoietin-2 (Ang-2) (rabbit polyclonal; Proteintech, Rosemont, IL, USA). After several washes, the samples were incubated for 2 h at RT with the following secondary antibodies: Cy3-conjugated goat anti-Armenian hamster IgG, Cy3-conjugated donkey anti-mouse IgG, Cy3-conjugated donkey anti-rabbit IgG, FITC-conjugated goat anti-Armenian hamster IgG (all from Jackson ImmunoResearch, West Grove, PA, USA). Nuclei were stained with 4′6-diamidino-2-phenylindole. The samples were then mounted in Fluorescent Mounting Medium (Dako, Carpinteria, CA, USA) and immunofluorescent images were acquired using a laser-scanning confocal microscope (LSM 880 with Airyscan; Carl Zeiss, Jena, Germany).

2.4. Morphometric analysis

Density measurement of blood vessels and metastasis were performed with ImageJ software (http://rsb.info.nih.gov/ij). For blood vessel density, $CD31^+$ area per random 0.42 mm^2 areas was measured in the peri- and intratumoral regions. The numbers of blood vessels > 100 μm were measured in the random 0.42 mm^2 peri- and intratuoral areas. To determine the amount of Ang-2 expression, $Ang\text{-}2^+$ area in random 0.42 mm^2 area were calculated in the peri- and intratumoral regions. In addition, coverage of $\alpha\text{-SMA}^+$ mural cells was calculated as the percentage of corresponding fluorescent positive length along the $CD31^+$ vessels in random 0.42 mm^2 in the peri- and intratumoral regions. As for the quantification of lymph nodes metastasis, cytokeratin + area per random 0.42 mm^2 was calculated in the cortex and medulla regions. For apoptosis analyses, $cleaved\text{-}caspase\text{-}3^+$ area per random 0.42 mm^2 area was measured in both B16F10 cells and tumor tissues.

2.5. Cell culture and reagents

HUVECs and their growth medium (EGM-2 MV BulletKit™) were purchased from Lonza Group Ltd. (Basel, Switzerland). The cells were used at passage 4–5 in all experiments. B16F10 cells were cultured in Dulbecco's modified Eagle's medium (Gibco, Grand Island, NY, USA) supplemented with 10% fetal bovine serum (Atlas Biologicals, For Collins, CO, USA), 100 U/ml penicillin and 100 μg streptomycin (Sigma-Aldrich). All cells were incubated at 37 °C with 5% CO_2. Diosmetin was dissolved in dimethyl sulfoxide to obtain a 10 mg/ml (for *in vitro* use) or 1 mg/ml (for *in vivo* use) stock solution, which was then diluted with autoclaved PBS prior to use.

2.6. Cell proliferation assays

Cell proliferation was determined by a 3-(4,5-dimethylthiazol-2-yl)-2,5-diphenyltetrazolium bromide (MTT) assay. B16F10 cells were seeded in 24-well plates (1×10^5 cells/well) overnight and treated with or without diosmetin. After 24 h, the media was carefully removed and 300 μl of MTT solution (0.5 mg MTT/ml medium) was added to each well, and plates were incubated for 2 h at 37 °C. The media was then replaced with 500 μl of dimethyl sulfoxide, and the plates were shaken for 10 min. Then, 200 μl of the sample were transferred to a 96-well microplate. The results were quantified by measuring the absorbance at 570 nm with a microplate reader (Spectramax M2; Molecular Devices, CA, USA).

2.7. Lactate dehydrogenase (LDH) release assays

LDH levels released from damaged cells into the culture medium were measured using a cytotoxicity detection kit (Takara Bio Inc., Shiga, Japan) according to the manufacturer's instructions. Briefly, B16F10 cells were seeded in 24-well plates (1×10^5 cells/well) overnight and treated with or without diosmetin for 24 h. After treatment, culture medium was collected and centrifuged at 250 × *g* for 10 min to remove the debris. The supernatant was collected and incubated with the LDH reaction mixture at RT for 30 min in dark condition. Released LDH level was determined at 490 nm in microplate reader (Molecular Devices).

2.8. Annexin V assay

Cell apoptosis was assessed by the Annexin V assay (Santa Cruz

Biotechnology, Inc., Dallas, TX, USA) according to the manufacturer's protocol using a flow cytometry method. Annexin V content was determined by measuring fluorescence at 488 nm (excitation) and 525 nm (emission) using a Guava easyCyte^{HT} system (Millipore, Billerica, MA, USA).

2.9. In vitro migration assays

B16F10 cells and HUVECs were grown on 6-well plates. Confluent monolayer cells were scratched manually using a sterile 1000 µl pipette tip and gently washed with PBS. Fresh medium containing 2% fetal bovine serum was added to the wells with different concentrations of diosmetin. At the indicated time after treatment, images were photographed using a microscope (Nikon Eclipse TS100; Nikon Corporation, Tokyo, Japan).

2.10. In vitro tube formation assays

For ECs tube formation assay, growth factor reduced Matrigel™ (Corning Inc., NY, USA) was thawed overnight at 4 °C. The Matrigel was allowed to solidify on a 24-well culture plate at 37 °C for 30 min. HUVECs were harvested and seeded at a density of 1×10^5 cells/well in growth media with or without diosmetin. Cells were then incubated at 37 °C for a further 18 h. Tube formation was observed by taking pictures using a microscope (Nikon Corporation). The tube formation assays were quantified by counting the number of tubules from three different fields for each condition.

2.11. Rat aortic ring assays

For *ex-vivo* angiogenesis study, the rat aortic ring assay was used following a published protocol with modificiations [31]. Briefly, the thoracic aorta from a freshly sacrificed Sprague-Dawley rats (4-week-old, Samtako) was removed in a sterile manner and rinsed in ice cold PBS. It was then cut into 1 mm long pieces using surgical blade. Each ring was placed in a matrigel pre-coated 24-well-plate. Dulbecco's modified Eagle's medium containing 10% fetal bovine serum was added to the wells with or without diosmetin. Seven days after treatment, the rings were analyzed by microscope (Nikon Corporation) and microvessels sprouting were quantified.

2.12. Western blotting

At the indicated time, B16F10 cells were homogenized in ice-cold lysis buffer containing a protease inhibitor cocktail (Sigma-aldrich). Each protein was separated with SDS-PAGE and transferred to nitrocellulose membranes. After blocking with 5% skim milk, the membranes were incubated with the following primary antibodies in blocking buffer overnight at 4 °C: anti-caspase-3 (rabbit), anti-Poly (ADP-ribose) polymerase (PARP) (rabbit; both from Cell Signaling Technology, Inc., Beverly, MA, USA), and anti-β-actin (mouse monoclonal; Sigma-Aldrich). Membranes were then incubated with HRP-conjugated secondary antibodies for 1 h at RT. Chemiluminescent signals were developed with HRP substrate (Millipore) and detected with a Fusion FX7 acquisition system (Vilbert Lourmat, Eberhardzell, Germany).

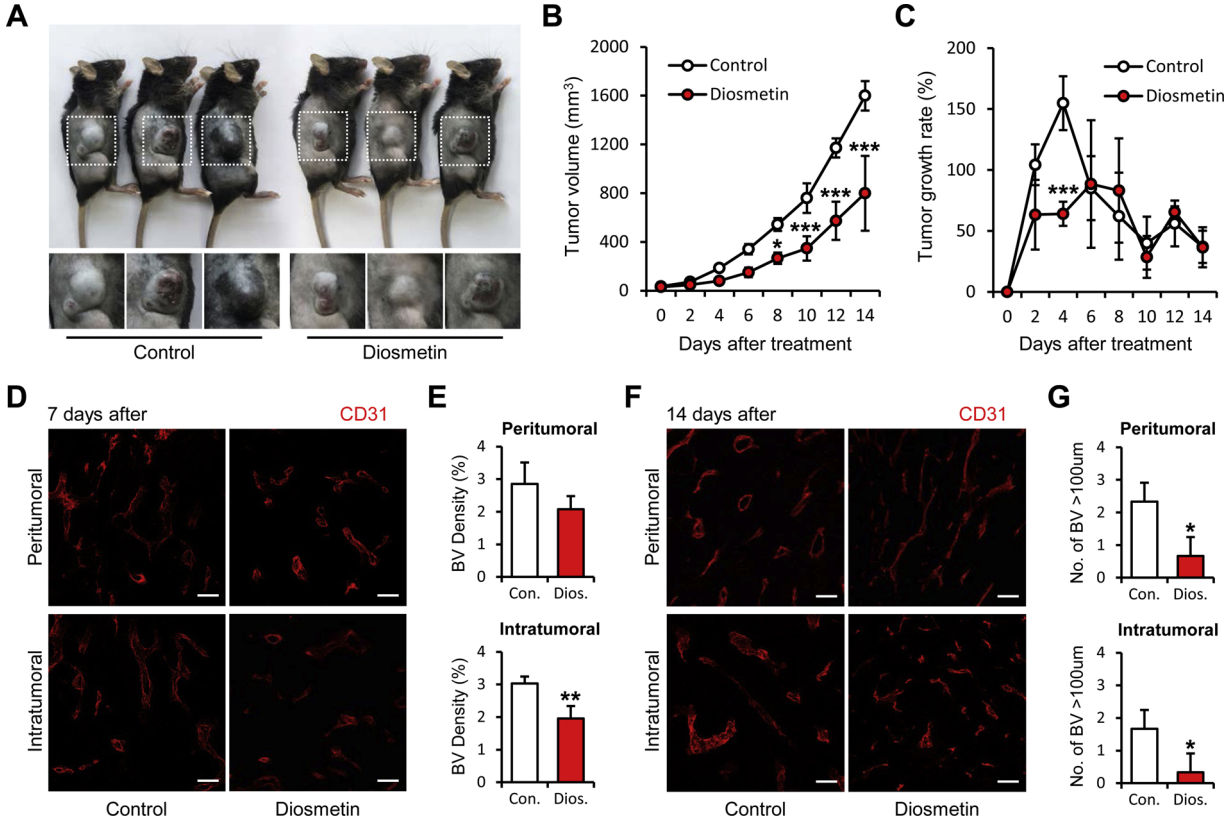

Fig. 1. Anti-cancer effects of diosmetin by inhibiting tumor angiogenesis *in vivo*.
(A) Images showing tumor development seven days after treatment. The magnified images demarcate melanoma tumor masses. Each group: n = 10. (B, C) Comparison of the tumor volume and tumor growth rate. (D, E) Images and quantification of blood vessels density seven days after treatment in the peri- and intratumoral regions. (F, G) Images and quantification of No. of tumor vessels with a size > 100 µm 14 days after treatment in the peri- and intratumoral regions. Unless otherwise denoted: scale bar, 100 µm. n = 5 for each group. Values are mean ± SD. $^*P < 0.05$; $^{**}P < 0.01$; $^{***}P < 0.001$ *versus* untreated mice.

2.13. Immunocytochemistry

B16F10 cells and HUVECs were cultured on glass coverslips coated with 0.1% gelatin. Cells were fixed with cold 2% paraformaldehyde and permeabilized with ice cold 0.5% Triton X-100 in PBS for 5 min and blocked in 5% donkey (or goat) serum in 0.3% TritonX-100 in PBS for 1 h at RT. The cells were incubated with anti-caspase-3 (rabbit polyclonal; R&D Systems) and anti-Ang-2 (rabbit polyclonal; Proteintech) antibodies overnight at 4 °C. Cells were incubated with Cy3-conjugated donkey anti-rabbit IgG (Jackson ImmunoResearch). Nuclei were stained with 4′6-diamidino-2-phenylindole. Then, the cells were mounted in Fluorescent Mounting Medium (Dako) and immunofluorescent images were acquired using a confocal microscope (Carl Zeiss).

2.14. Statistical analysis

Values are presented as the mean ± standard deviation (SD). Significant differences between groups were determined by unpaired Student t-tests. For multigroup analysis of variances, one-way or two-way ANOVA was performed followed by Bonferroni post-tests. Statistical significance was set as < 0.05 and indicated as $^{*}P < 0.05$, $^{**}P < 0.01$, and $^{***}P < 0.001$.

3. Results

3.1. Diosmetin delays tumor growth by inhibiting tumor-induced angiogenesis

To investigate the effect of diosmetin on tumor growth, we generated a mouse melanoma model by subcutaneously injecting B16F10 cells into C57BL/6 mice. A week after implantation, the mice were randomly divided into two groups: one group was treated with diosmetin, the other received no treatment and was used as a control. Representative images showed diosmetin remarkably suppressed tumor growth in mice (Fig. 1a). 14 days after treatment, diosmetin-treated mice showed a 50% reduction in tumor growth compared to untreated mice (Fig. 1b), and the most significant inhibition was observed five days after treatment (Fig. 1c).

To examine the effect of diosmetin on tumor vasculature, we performed immunostaining with anti-CD31 (endothelial cell [EC]-specific)

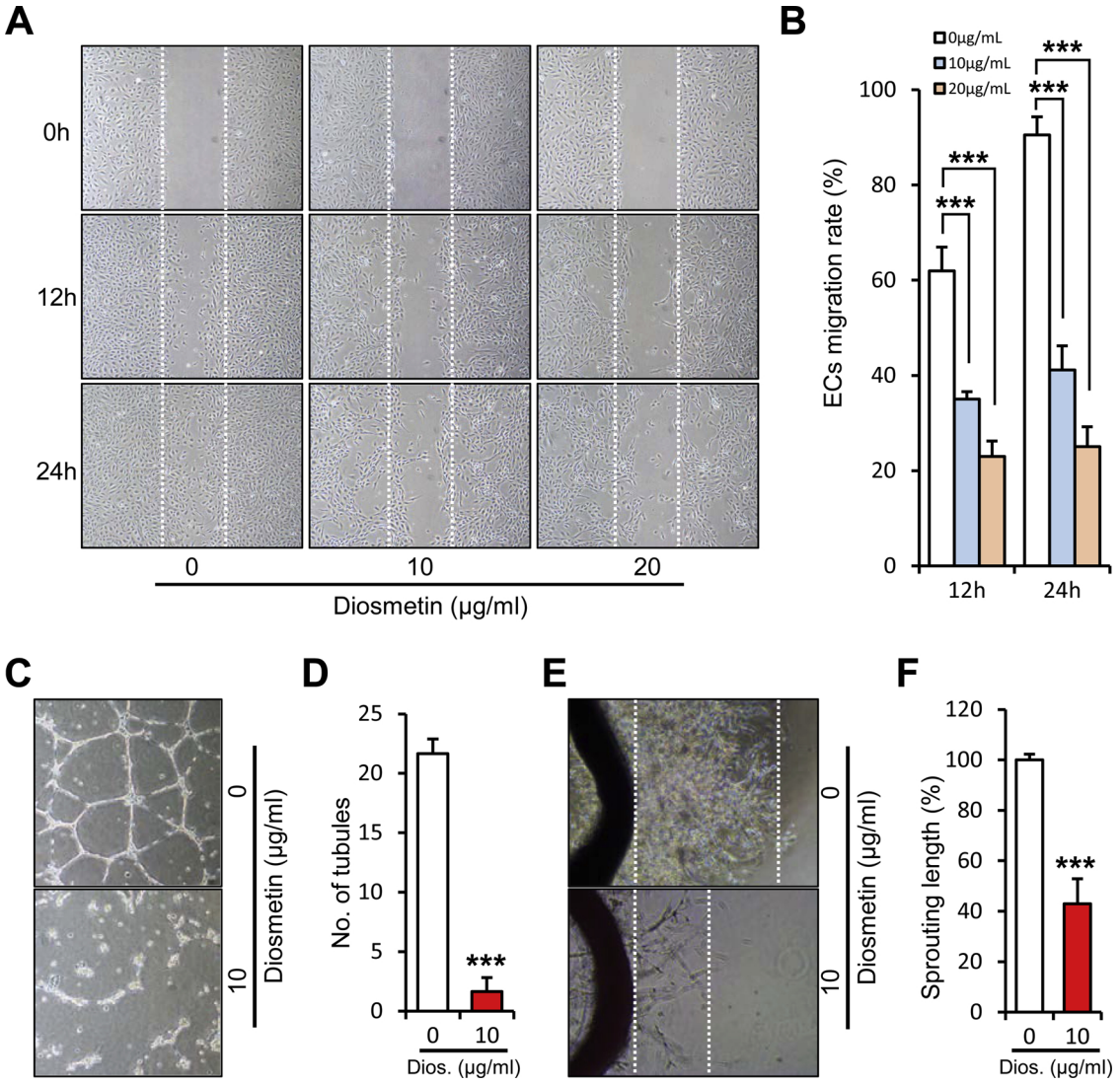

Fig. 2. Diosmetin inhibits angiogenesis *in vitro* and *ex vivo*.
(A, B) Images showing ECs migration and comparisons of ECs migration. Data are presented as a percentage of scratched area at time 0 h. (C, D) Images showing ECs tube formation and comparisons of number of tubules. (E, F) Images showing sprouting of ECs from rat aorta and comparisons of maximal length of ECs sprouting. The data are presented as percentage of untreated group. Unless otherwise denoted: magnification, 40 × . Values are mean ± SD from ≥ three independent experiments. $^{***}P < 0.001$ *versus* untreated group.

antibodies. Seven days after treatment with diosmetin, compared with untreated mice, blood vessels density decreased in diosmetin-treated mice, particularly in the intratumoral region (Fig. 1d, e). Interestingly, 14 days after treatment, tumor vessels with a size > 100 μm were predominantly observed in the tumors of untreated mice. In contrast, diosmetin treatment significantly reduced the blood vessels' size in the tumor (Fig. 1f, g). These results showed that diosmetin delays tumor growth by inhibiting vascular sprouting and enlargement during tumor progression.

3.2. Diosmetin inhibits ECs migration, tube formation and microvessels sprouting

To further study the inhibitory effect of diosmetin on angiogenesis, we performed cell migration assays, ECs tube formation assays on Matrigel, and *ex vivo* aorta ring assays. In migration assays, we found that diosmetin significantly suppressed the migration of ECs in a dose- and time-dependent manner. Control cells started to migrate into the scratch area, and almost completely filled it after 24 h. However, 12 h after the scratch, ECs treated with 10 or 20 μg/ml diosmetin had migrated less than control cells (35.0% and 22.9% *vs.* 61.9%), and the decreased mobility of the treated ECs was more evident 24 h after the scratch (treated cells migrated 41.1% and 25.0%, control cells migrated 90.4%) (Fig. 2a, b). Furthermore, *in vitro* tube formation assays showed that diosmetin almost completely disrupted the tubule formation of HUVECs (Fig. 2c, d). To determine the potential effect of diosmetin on microvessels sprouting *ex vivo*, we performed rat aortic ring assays. We found that diosmetin inhibited microvessels sprouting from the aortic rings, and reduced sprouting length by more than 50% compared to control (Fig. 2e, f). These results indicated that diosmetin has an anti-angiogenic effect against sprouting and formation of new vessels.

3.3. Diosmetin induces normalization of tumor vasculature, resulting in suppression of metastasis

To address the alteration of tumor vasculature following treatment with diosmetin, tumor tissues were separated from diosmetin-treated or untreated mice and immunostained with anti-Ang-2 (proangiogenic factor-specific) and anti-α-SMA (pericyte-specific) antibodies. Ang-2 expression in diosmetin-treated mice was lower than in untreated mice and the lowest levels of Ang-2 were observed in the intratumoral regions, which are hypoxic. In contrast, tumors in untreated mice showed similar Ang-2 expression thorough (Fig. 3a, b). Furthermore, high expression of α-SMA was observed in diosmetin-treated mice. Diosmetin increased the pericyte coverage of tumor blood vessels more than two and three times compared with the peri- and intratumoral regions, respectively, of untreated mice (Fig. 3c, d). These results showed that diosmetin induces tumor vessel normalization by downregulating Ang-2 and enhancing pericyte coverage.

To confirm the anti-metastatic effect of diosmetin *in vivo*, we harvested lungs and inguinal lymph nodes of the melanoma-bearing mice. The representative images showed that diosmetin markedly blocked spontaneous metastasis to lungs compared with untreated mice. H&E staining further verified that melanoma lung colonies were observed only in the untreated mice (Fig. 3e). Additionally, the immunostaining with anti-cytokeratin (tumor cell-specific) and LYVE-1 (lymphatic vessel-specific) antibodies showed that diosmetin significantly reduced lymph nodes metastasis in both the cortex and medullar regions. In

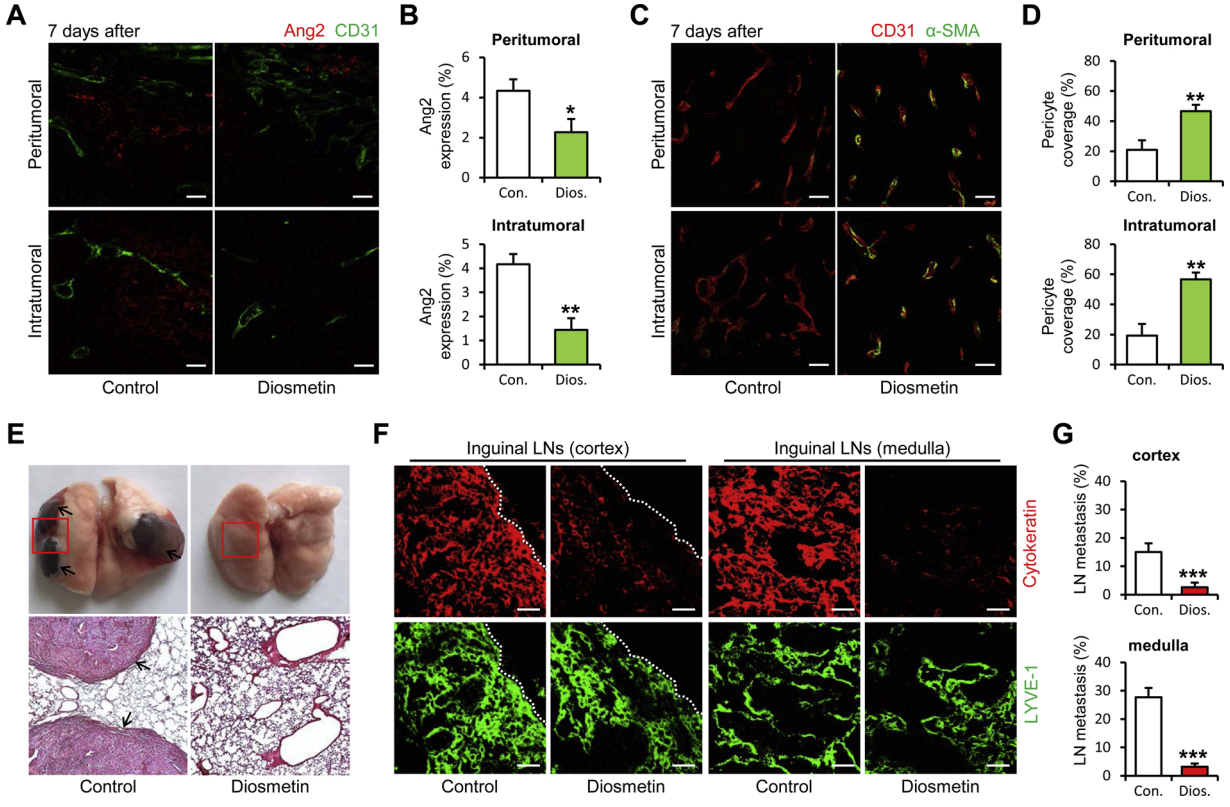

Fig. 3. Diosmetin induces normalization of tumor vessels and suppresses spontaneous metastasis to lungs and inguinal LNs.
(A, B) Images and quantification of Ang-2$^+$ area in the peri- and intratumoral regions. (C, D) Images and quantification of α-SMA + mural cell coverage on tumor vessels. (E) Images showing spontaneous metastasis in lungs and H&E stained lung sections are viewed metastatic regions under higher magnification (lower panels). Arrows indicate metastatic colonies. Magnification 100 × . (F, G) Images and quantification of cytokeratin$^+$ tumor metastasis in the Inguinal lymph nodes. Dotted lines indicate the margin of inguinal lymph node. Unless otherwise denoted: scale bar, 100 μm. n = 5 for each group. Values are mean ± SD. *P < 0.05; **P < 0.01; ***P < 0.001 *versus* untreated mice.

untreated mice, the metastasis rate was 15% and 27% in the cortex and medulla, respectively. By contrast, in diosmetin-treated mice, the metastasis rate was 2.6% and 3.1% in the same regions (Fig. 3f, g). These results indicated that diosmetin suppresses spontaneous metastasis formation to lungs and inguinal lymph nodes.

3.4. Diosmetin suppresses melanoma cells proliferation and migration

To assess the anti-proliferative effect of diosmetin on B16F10 cells, morphological observations, MTT and LDH assays were performed. The representative images showed that melanoma cells became more elongated after diosmetin treatment in a dose-dependent manner (Fig. 4a). Diosmetin significantly decreased cell proliferation upon concentration at 10 and 20 μg/ml by 59.5% and 62.2%, respectively (Fig. 4b). Additionally, diosmetin exerted remarked tumor cell cytotoxicity in a dose-dependent manner (Fig. 4c). To assess the inhibitory effect of diosmetin on the migration of tumor cells, we performed scratch assays. Diosmetin remarkably inhibited B16F10 cells migration in a dose-dependent manner. After 12 h, the migration rate of B16F10 cells treated with diosmetin at 1 and 10 μg/ml was significantly reduced by 18.6% and 76.5%, respectively, compared with untreated cells. After 24 h, the scratch area in the untreated cells was almost covered with cells, whereas the gap in diosmetin-treated cells remained. The migration rate of the cells treated with diosmetin at 1 and 10 μg/ml decreased to 27.2% and 73.9%, respectively, compared to untreated cells (Fig. 4d, e).

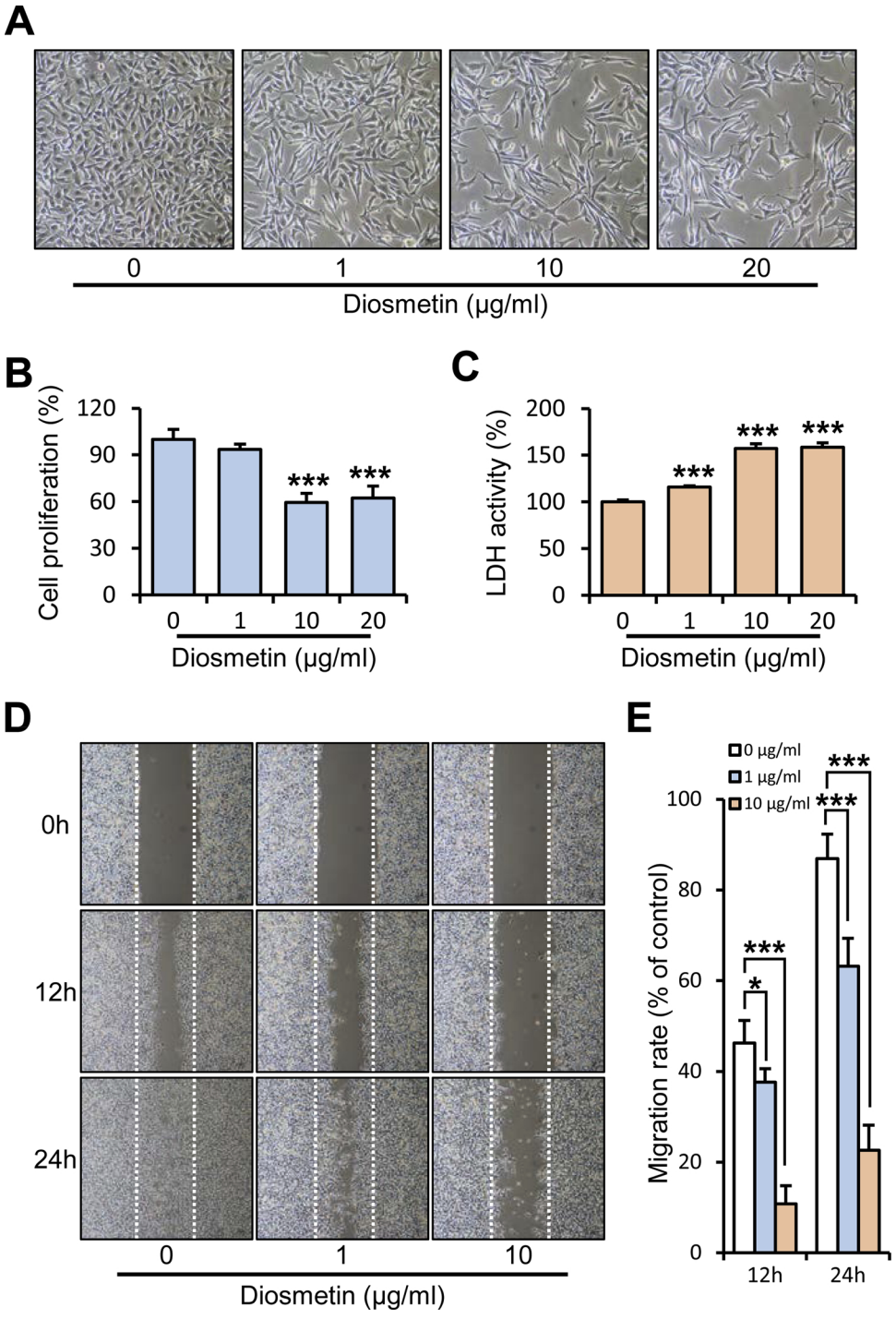

Fig. 4. Inhibitory effect of diosmetin on the tumor cell proliferation and migration.
(A) Images showing morphological changes on B16F10 melanoma cells after diosmetin-treatment in a dose-dependent manner. (B, C) Comparisons of B16F10 cells proliferation and cytotoxicity. (D, E) Images showing B16F10 cells migration after diosmetin-treatment in a dose- or time-dependent manner and comparisons of the cells migration rate. Migration rate of B16F10 cells is presented as a percentage of scratched area at time 0 h. Unless otherwise denoted: magnification, 40 ×. Values are mean ± SD from ≥ three independent experiments. $^{*}P < 0.05$; $^{***}P < 0.001$ *versus* untreated group.

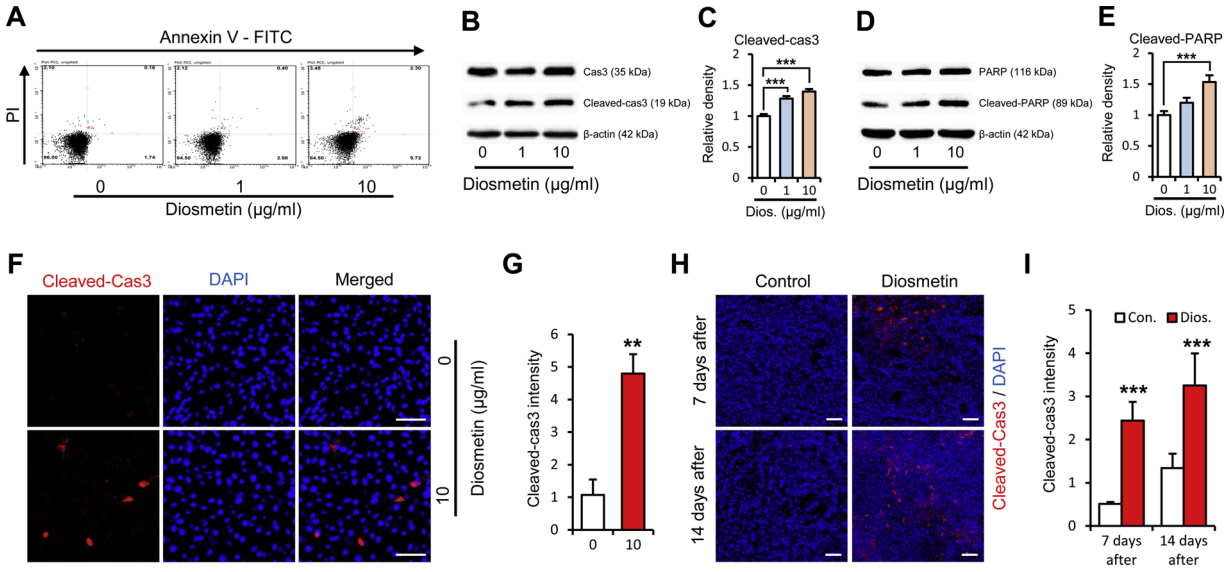

Fig. 5. Diosmetin induces cell apoptosis by activating caspase-3.
(A) Apoptosis in B16F10 cells was measured by flow cytometry with Annexin V-FITC staining. Values are mean ± SD from ≥ three independent experiments. (B–E) Immunoblotting showing expression of caspase-3, cleaved-caspase-3 and PARP, cleaved-PARP after diosmetin-treatment in a dose-dependent manner. Values are mean ± SD from ≥ three independent experiments. (F–I) Images and quantification of cleaved-caspase-3$^+$ area in B16F10 cells and tumor tissues. Unless otherwise denoted: scale bar, 100 μm. n = 5 for each group. Values are mean ± SD. $^{**}P < 0.01$; $^{***}P < 0.001$ *versus* untreated mice.

3.5. Diosmetin induces melanoma cells apoptosis via the activation of caspase-3

To elucidate how diosmetin inhibits tumor cell growth, we evaluated its effects on the apoptosis of B16F10 cells. Following treatment with 1 and 10 μg/ml diosmetin, the percentage of apoptotic cells increased compared with that in control cells (2.98% and 9.72% *vs.* 1.74%, respectively; Fig. 5a). Western blot analysis demonstrated that diosmetin significantly induced the activation of caspase-3 through its cleavage (Fig. 5b, c) and upregulated the expression of cleaved-PARP (Fig. 5d, e) in a dose-dependent manner. The activation of caspase-3 upon diosmetin treatment was confirmed by immunofluorescence staining in both B16F10 cells and tumor tissues (Fig. 5f-i). These results indicated that diosmetin induces B16F10 cell apoptosis *via* activation of caspase-3, leading to inhibition of the tumor cell growth.

4. Discussion

Malignant melanoma is the most aggressive skin cancer that tend to metastasize to other organs. Chemotherapy commonly used to combat cutaneous melanoma that cannot be treated by surgery only. But current chemotherapies have limited efficacy and caused severe side effects [32]. Therefore, research has focused on the identification of effective and safe anti-cancer drugs from natural products. Diosmetin is a dietary flavone, whose antitumor activity has been demonstrated in many types of cancers [14–17]. However, there have been no reports determining the anti-cancer effect of diosmetin in melanoma. In this study, for the first time, we demonstrated that diosmetin exerts anti-cancer effects on melanoma directly or indirectly. Our results showed that diosmetin had an inhibitory effect on tumor angiogenesis; caused tumor vasculature normalization and metastasis suppression in lung and lymph node metastases; and induced melanoma cell death by apoptosis.

Cancer cells induce angiogenesis to support their rapid proliferation [20]. Several studies have shown that citrus flavonoids exhibit anti-angiogenic activities *in vitro* and *in vivo*. Nobiletin, a citrus poly-methoxyflavonoid, has been found to suppress not only proliferation, migration and tube formation on HUVECs, but also embryonic angiogenesis in a chick embryo chorioallantoic membrane system [33]. Another citrus flavonoid, Gold Lotion, possesses anti-cancer properties by inhibiting the expression of VEGF and COX-2 in skin cancer [34]. In this study, we demonstrated that diosmetin plays a critical role in inhibiting angiogenesis both *in vivo* and *in vitro*. Diosmetin delayed tumor growth by suppressing tumor-angiogenesis in a murine melanoma model. Notably, diosmetin potently exerted its inhibitory effect on capillary enlargement in the late stage of tumor progression, and significantly disrupted blood vessel sprouting in the early stage. Furthermore, we also confirmed that diosmetin suppressed microvessels growth and branching in *ex vivo* rat aorta ring assays and blocked angiogenesis by inhibiting endothelial cell migration and tube formation. These results show that diosmetin exhibits a potent inhibitory effect on angiogenesis, leading to suppression of tumor growth.

The immature and destabilized tumor vasculature results in tumor progression, metastatic dissemination to other tissues and insufficient therapeutic drug delivery [22]. The dysfunctionality of the tumor vessels is associated with abnormal levels of growth factors, such as angiopoietins [20]. Among them, Ang-2 has been reported to act as an antagonist for Ang-1 and is involved in the destabilization of ECs-pericyte interactions [35,36]. Therefore, inhibition of Ang-2 may have a key role in tumor vessel normalization and enhancement of drug delivery into the tumor core region. Our results showed that diosmetin significantly downregulated Ang-2 expression in the whole tumor. In addition, the pericyte coverage in diosmetin-treated tumor vessels was greater than that in untreated tumor vessels. Particularly, in the intratumoral region, diosmetin not only considerably suppressed Ang-2 expression but also remarkably enhanced ECs-pericyte interaction. Because it is difficult to deliver drugs into the center of tumor through impaired tumor vasculature, this effect of diosmetin on vascular structure is particularly attractive. Moreover, our data showed that tumor vessels normalization by diosmetin led to complete suppression of metastasis formation in lungs and inguinal lymph nodes. According to a recent study, diosmetin inhibits metastasis formation by down-regulating the MMP-2 and MMP-9 expression [37]. Our results suggested a different strategy to suppress metastasis: diosmetin normalized abnormal tumor vasculature by improving ECs-pericyte interactions through the downregulation of Ang-2 expression (Fig. 6).

A cancer therapy targeting apoptosis is highly effective and the most successful non-surgical method in cancer treatment [38]. Thus,

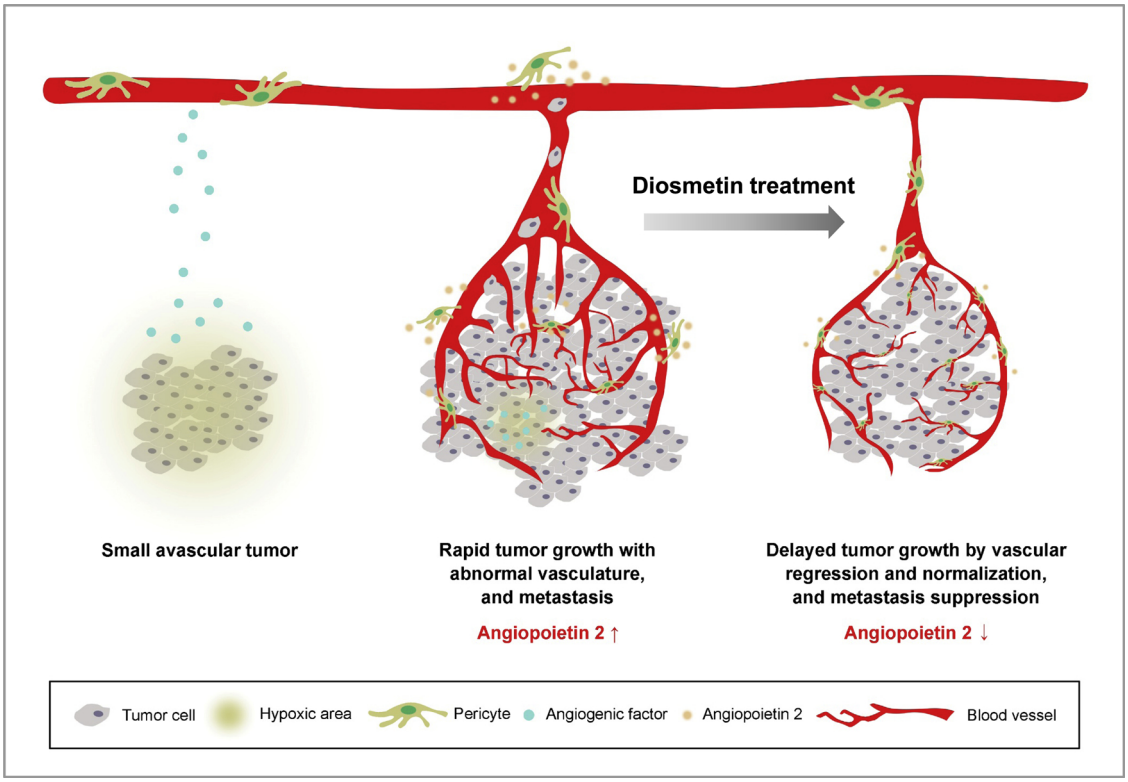

Fig. 6. Schematic diagram of anti-cancer effect of diosmetin-treatment during tumor progression.

targeting regulators of apoptosis has been considered a promising strategy for different types of cancer, including melanoma [39]. Previous studies have shown that diosmetin induces tumor cell apoptosis by activating the p53/Bcl-2 pathway [40,41]. In our study, we confirmed that diosmetin elicited tumor cell death *via* apoptosis. Diosmetin significantly inhibited B16F10 cell proliferation and migration in a dose-dependent manner. Diosmetin increased both the activation of caspase-3, an executioner caspase in apoptosis, and that of its downstream substrate PARP in a dose-dependent manner. Immunostaining assays confirmed this result, showing that diosmetin treatment resulted in increased expression of cleaved-caspase-3 in melanoma tissues *in vivo* and in B16F10 cells *in vitro*. Finally, the increased expression of cleaved-caspase-3 and cleaved-PARP lead to cell death.

In conclusion, our data demonstrate that diosmetin exerts a potent anti-cancer activity by inducing vascular regression, normalization, and cell apoptosis, resulting in the delay of tumor growth and inhibition of metastasis formation. Notably, because diosmetin induces normalization of tumor vasculature, our results strongly suggest that diosmetin is a promising adjuvant as a combination treatment drug to enhance the efficacy of conventional chemotherapy.

Declaration of Competing Interest

The authors declare that they have no conflict of interest.

Acknowledgments

This work was supported by Korea Institute of Planning and Evaluation for Technology in Food, Agriculture, Forestry (IPET) through Agriculture, Food and Rural Affairs Research Center Support Program, funded by Ministry of Agriculture, Food and Rural Affairs (MAFRA; 716002-7)

References

[1] A.M. Eggermont, A. Spatz, C. Robert, Cutaneous melanoma, Lancet 383 (2014) 816–827.
[2] C. Garbe, K. Peris, A. Hauschild, P. Saiag, M. Middleton, A. Spatz, J.-J. Grob, J. Malvehy, J. Newton-Bishop, A. Stratigos, Diagnosis and treatment of melanoma: european consensus-based interdisciplinary guideline, Eur. J. Cancer 46 (2010) 270–283.
[3] J. Ferlay, I. Soerjomataram, R. Dikshit, S. Eser, C. Mathers, M. Rebelo, D.M. Parkin, D. Forman, F. Bray, Cancer incidence and mortality worldwide: sources, methods and major patterns in GLOBOCAN 2012, Int. J. Cancer 136 (2015) E359–E386.
[4] J. Ferlay, I. Soerjomataram, M. Ervik, R. Dikshit, S. Eser, C. Mathers, M. Rebelo, D. Parkin, D. Forman, F. Bray, Cancer incidence and mortality worldwide: IARC CancerBase, GLOBOCAN v10, (11) (2012).
[5] C. Williams, C. Quirk, A. Quirk, Melanoma: a new strategy to reduce morbidity and mortality, Australas. Med. J. 7 (2014) 266.
[6] H. Liu, L. Lv, K. Yang, Chemotherapy targeting cancer stem cells, Am. J. Cancer Res. 5 (2015) 880.
[7] S. Roowi, A. Crozier, Flavonoids in tropical citrus species, J. Agric. Food Chem. 59 (2011) 12217–12225.
[8] M. Mueller, B. Lukas, J. Novak, T. Simoncini, A.R. Genazzani, A. Jungbauer, Oregano: a source for peroxisome proliferator-activated receptor γ antagonists, J. Agric. Food Chem. 56 (2008) 11621–11630.
[9] L. Bıtıs, S. Kultur, G. Melıkoglu, N. Ozsoy, A. Can, Flavonoids and antioxidant activity of Rosa agrestis leaves, Nat. Prod. Res. 24 (2010) 580–589.
[10] N. AlGamdi, W. Mullen, A. Crozier, Tea prepared from Anastatica hirerochuntica seeds contains a diversity of antioxidant flavonoids, chlorogenic acids and phenolic compounds, Phytochemistry 72 (2011) 248–254.
[11] B.C. Chan, M. Ip, H. Gong, S. Lui, R.H. See, C. Jolivalt, K. Fung, P. Leung, N.E. Reiner, C.B. Lau, Synergistic effects of diosmetin with erythromycin against ABC transporter over-expressed methicillin-resistant Staphylococcus aureus (MRSA) RN4220/pUL5054 and inhibition of MRSA pyruvate kinase, Phytomedicine 20 (2013) 611–614.
[12] D. Chandler, A. Woldu, A. Rahmadi, K. Shanmugam, N. Steiner, E. Wright, O. Benavente-García, O. Schulz, J. Castillo, G. Münch, Effects of plant-derived polyphenols on TNF-α and nitric oxide production induced by advanced glycation endproducts, Mol. Nutr. Food Res. 54 (2010) S141–S150.
[13] W. Liao, Z. Ning, L. Chen, Q. Wei, E. Yuan, J. Yang, J. Ren, Intracellular antioxidant detoxifying effects of diosmetin on 2, 2-azobis (2-amidinopropane) dihydrochloride (AAPH)-induced oxidative stress through inhibition of reactive oxygen species generation, J. Agric. Food Chem. 62 (2014) 8648–8654.
[14] V.P. Androutsopoulos, S. Mahale, R.R. Arroo, G. Potter, Anticancer effects of the flavonoid diosmetin on cell cycle progression and proliferation of MDA-MB 468 breast cancer cells due to CYP1 activation, Oncol. Rep. 21 (2009) 1525–1528.

[15] R. Zhao, Z. Chen, G. Jia, J. Li, Y. Cai, X. Shao, Protective effects of diosmetin extracted from Galium verum L. On the thymus of U14-bearing mice, Can. J. Physiol. Pharmacol. 89 (2011) 665–673.
[16] V.P. Androutsopoulos, D.A. Spandidos, The flavonoids diosmetin and luteolin exert synergistic cytostatic effects in human hepatoma HepG2 cells via CYP1A-catalyzed metabolism, activation of JNK and ERK and P53/P21 up-regulation, J. Nutr. Biochem. 24 (2013) 496–504.
[17] J. Liu, H. Ren, B. Liu, Q. Zhang, M. Li, R. Zhu, Diosmetin inhibits cell proliferation and induces apoptosis by regulating autophagy via the mammalian target of rapamycin pathway in hepatocellular carcinoma HepG2 cells, Oncol. Lett. 12 (2016) 4385–4392.
[18] J. Folkman, Role of angiogenesis in tumor growth and metastasis, Semin. Oncol. 29 (2002) 15–18.
[19] D. Dewing, M. Emmett, R. Pritchard Jones, The roles of angiogenesis in malignant melanoma: trends in basic science research over the last 100 years, ISRN Oncol. (2012).
[20] P. Carmeliet, R.K. Jain, Molecular mechanisms and clinical applications of angiogenesis, Nature 473 (2011) 298.
[21] D. Hanahan, R.A. Weinberg, Hallmarks of cancer: the next generation, cell 144 (2011) 646–674.
[22] P. Carmeliet, R.K. Jain, Principles and mechanisms of vessel normalization for cancer and other angiogenic diseases, Nat. Rev. Drug Discov. 10 (2011) 417.
[23] J.A. Nagy, S.-H. Chang, S.-C. Shih, A.M. Dvorak, H.F. Dvorak, Heterogeneity of the tumor vasculature, Seminars in thrombosis and hemostasis, NIH Public Access (2010) 321.
[24] C. Kim, H. Yang, Y. Fukushima, P.E. Saw, J. Lee, J.-S. Park, I. Park, J. Jung, H. Kataoka, D. Lee, Vascular RhoJ is an effective and selective target for tumor angiogenesis and vascular disruption, Cancer Cell 25 (2014) 102–117.
[25] A.S. Chung, N. Ferrara, Developmental and pathological angiogenesis, Annu. Rev. Cell Dev. Biol. 27 (2011) 563–584.
[26] C. Viallard, B. Larrivée, Tumor angiogenesis and vascular normalization: alternative therapeutic targets, Angiogenesis 20 (2017) 409–426.
[27] J.M. Ebos, R.S. Kerbel, Antiangiogenic therapy: impact on invasion, disease progression, and metastasis, Nat. Rev. Clin. Oncol. 8 (2011) 210.
[28] R.K. Jain, Normalization of tumor vasculature: an emerging concept in anti-angiogenic therapy, Science 307 (2005) 58–62.
[29] R.K. Jain, Normalizing tumor vasculature with anti-angiogenic therapy: a new paradigm for combination therapy, Nat. Med. 7 (2001) 987.
[30] R.K. Jain, Antiangiogenesis strategies revisited: from starving tumors to alleviating hypoxia, Cancer Cell 26 (2014) 605–622.
[31] S. Saraswati, S. Agrawal, Brucine, an indole alkaloid from Strychnos nux-vomica attenuates VEGF-induced angiogenesis via inhibiting VEGFR2 signaling pathway in vitro and in vivo, Cancer Lett. 332 (2013) 83–93.
[32] B. Domingues, J.M. Lopes, P. Soares, H. Pópulo, Melanoma treatment in review, Immunotargets Ther. 7 (2018) 35.
[33] K. Kunimasa, M. Ikekita, M. Sato, T. Ohta, Y. Yamori, M. Ikeda, S. Kuranuki, T. Oikawa, Nobiletin, a citrus polymethoxyflavonoid, suppresses multiple angiogenesis-related endothelial cell functions and angiogenesis in vivo, Cancer Sci. 101 (2010) 2462–2469.
[34] M.-H. Pan, S. Li, C.-S. Lai, Y. Miyauchi, M. Suzawa, C.-T. Ho, Inhibition of citrus flavonoids on 12-O-tetradecanoylphorbol 13-acetate-induced skin inflammation and tumorigenesis in mice, Food Sci. Hum. Wellness 1 (2012) 65–73.
[35] T. Holopainen, P. Saharinen, G. D'amico, A. Lampinen, L. Eklund, R. Sormunen, A. Anisimov, G. Zarkada, M. Lohela, H. Heloterä, Effects of angiopoietin-2-blocking antibody on endothelial cell–cell junctions and lung metastasis, J. Natl. Cancer Inst. 104 (2012) 461–475.
[36] H.G. Augustin, G.Y. Koh, G. Thurston, K. Alitalo, Control of vascular morphogenesis and homeostasis through the angiopoietin–Tie system, Nat. Rev. Mol. Cell Biol. 10 (2009) 165.
[37] J. Liu, X. Wen, B. Liu, Q. Zhang, J. Zhang, H. Miao, R. Zhu, Diosmetin inhibits the metastasis of hepatocellular carcinoma cells by downregulating the expression levels of MMP-2 and MMP-9, Mol. Med. Rep. 13 (2016) 2401–2408.
[38] C. Pfeffer, A. Singh, Apoptosis: a target for anticancer therapy, Int. J. Mol. Sci. 19 (2018) 448.
[39] N. Mohana-Kumaran, D.S. Hill, J.D. Allen, N.K. Haass, Targeting the intrinsic apoptosis pathway as a strategy for melanoma therapy, Pigment Cell Melanoma Res. 27 (2014) 525–539.
[40] B. Liu, Y. Shi, W. Peng, Q. Zhang, J. Liu, N. Chen, R. Zhu, Diosmetin induces apoptosis by upregulating p53 via the TGF-β signal pathway in HepG2 hepatoma cells, Mol. Med. Rep. 14 (2016) 159–164.
[41] J. Qiao, J. Liu, K. Jia, N. Li, B. Liu, Q. Zhang, R. Zhu, Diosmetin triggers cell apoptosis by activation of the p53/Bcl-2 pathway and inactivation of the Notch3/NF-κB pathway in HepG2 cells, Oncol. Lett. 12 (2016) 5122–5128.